PHYSICAL REVIEW D **80,** 054005 (2009)

Real Compton scattering via color dipoles

B. Z. Kopeliovich,[1,2,*] Ivan Schmidt,[1,†] and M. Siddikov[1,‡]

[1]*Departamento de Física, Centro de Estudios Subatómicos, y Centro Científico-Tecnológico de Valparaíso, Universidad Técnica Federico Santa María, Casilla 110-V, Valparaíso, Chile*

[2]*Joint Institute for Nuclear Research, Dubna, Russia*

(Received 1 July 2009; published 8 September 2009)

We study the photoabsorption reaction and real Compton scattering within the color dipole model. We rely on a photon wave function derived in the instanton-vacuum model and on the energy-dependent phenomenological elastic dipole amplitude. Data for the photoabsorption cross section at high energies agree with our parameter-free calculations. We also provide predictions for the differential real Compton scattering cross section. Although no data for small angle Compton scattering are available so far, this process can be measured in ultraperipheral hadronic and nuclear collisions at the LHC.

DOI: 10.1103/PhysRevD.80.054005 PACS numbers: 13.60.Fz, 12.40.−y

I. INTRODUCTION

Compton scattering $\gamma + p \to \gamma + p$ and the related photoabsorption reaction have been a subject of intensive theoretical and experimental investigation [1–15]. While in the case of deeply virtual Compton scattering, where the initial photon is highly virtual, the QCD factorization is proven [5,7,8] and the amplitude can be expressed in terms of the generalized parton distributions (GPD) [1–15], in the case of real Compton scattering (RCS) the available theoretical tools are rather undeveloped.

On the one hand, it has been shown in Refs. [16,17] that, for large momentum transfer $\Delta_\perp$, it is possible to factorize the RCS amplitude [18,19] and express it in terms of the distribution amplitudes of the proton. On the other hand, it is possible to express the amplitude of the process via the minus 1st moment of GPDs at zero skewedness [5,20,21].

The traditional sources of quasireal and virtual photons, the electron beams, with very high collision energies are expected to be available in the near future. The new projects of the Large Hadron Electron Collider (LHeC) [22,23] and Electron Ion Collider (EIC) [24,25] are currently under intensive discussion. Besides the electron beams, one can also use beams of charged hadrons. Provided that the transverse overlap of the colliding hadrons is small, i.e. the transverse distance b between the colliding centers is larger than the sizes of the colliding particles $b > R_1 + R_2$, the electromagnetic interaction between colliding particles becomes the dominant mechanism. Such processes called ultraperipheral collisions can be studied in pp, pA, and AA collisions. In particular, one can access RCS in the reaction

$$A_1 + A_2 \to A_1 + \gamma + A_2. \tag{1}$$

The typical virtualities $\langle Q^2_{\gamma^*}\rangle$ of the intermediate photon γ^* are controlled by the form factors of the colliding particles and are small:

$$\langle Q^2_{\gamma^*}\rangle \lesssim \frac{3}{R_A^2} \sim \frac{0.1\ \mathrm{GeV}^2}{A^{2/3}}. \tag{2}$$

Thus, $\langle Q^2_{\gamma^*}\rangle$ is of the order of the soft hadronic scale, so the intermediate photon can be treated as a free Weizsäcker-Williams one; i.e. the amplitude of the process (1) can be described in terms of RCS.

These processes at the LHC will allow one to study RCS at very high energies. The possibility of the observation of such processes experimentally has been demonstrated by the STAR [26–28] and PHENIX [29] experiments at the Relativistic Heavy Ion Collider. It is expected that at the LHC photon-proton collisions at energies up to $\sqrt{s_{\gamma p}} \lesssim 8 \times 10^3$ GeV can be observed [30]. In this paper we concentrate on RCS on a proton target. Nuclear effects will be discussed elsewhere.

In what follows, we employ the color dipole approach introduced in Refs. [31,32]. The central objects of the model are the dipole scattering amplitude $\mathcal{A}(s, \beta, \vec{r})$ and the light-cone quark distribution functions of the photon. While perturbative QCD (pQCD) predicts the dipole amplitude only for small-size dipoles, several successful phenomenological parametrizations for the large-size dipoles are known. Relying on the photon wave function evaluated in the instanton-vacuum model [33], which is valid for any Q^2, one can extend the applicability of the model to the case of the processes with real photons [34]. In this paper, we are going to consider the real photoabsorption $\gamma + p \to X$ and the RCS.

II. COLOR DIPOLE MODEL

The color dipole model is valid only at sufficiently high energies, where the dominant contribution to the Compton amplitude comes from gluonic exchanges. Then the general expression for the Compton amplitude in the color dipole model has the form

*Boris.Kopeliovich@usm.cl
†Ivan.Schmidt@usm.cl
‡Marat.Siddikov@usm.cl

$$\mathcal{A}_{\mu\nu}(s,\Delta) \approx e_\mu^{(i)} e_\nu^{(j)} \int d\beta_1 d\beta_2 d^2r_1 d^2r_2 \bar{\Psi}_\gamma^{(i)}(\beta_2,\vec{r}_2) \times \mathcal{A}^d(\beta_1,\vec{r}_1;\beta_2,\vec{r}_2;\Delta)\Psi_\gamma^{(j)}(\beta_1,\vec{r}_1), \quad (3)$$

where $e_\mu^{(i)}$ is the photon polarization vector, $\beta_{1,2}$ are the light-cone fractional momenta of the quark and antiquark, $\vec{r}_{1,2}$ are the transverse distances in the final and initial dipoles, respectively, Δ is the momentum transfer in the Compton scattering, $\mathcal{A}^d(\ldots)$ is the scattering amplitude for the dipole state which also implicitly depends on s, c.m. energy squared, and $\Psi_\gamma^{(i)}(\beta_2,\vec{r}_2)$ is the wave function of the photon in the polarization state i [33].

At high energies in the small angle approximation $\Delta/\sqrt{s} \ll 1$, the quark separation and fractional momenta are preserved, so

$$\mathcal{I}m\mathcal{A}^d(\beta_1,\vec{r}_1;\beta_2,\vec{r}_2;\Delta) \approx \delta(\beta_1-\beta_2)\delta(\vec{r}_1-\vec{r}_2)\,\mathrm{Im} f_{\bar{q}q}^N(\vec{r}_1,\vec{\Delta},\beta_1). \quad (4)$$

Generally, the amplitude $f_{\bar{q}q}^N(\ldots)$ is a nonperturbative object, with asymptotic behavior for small r controlled by pQCD [31]:

$$f_{\bar{q}q}^N(\vec{r},\vec{\Delta},\beta) \sim r^2,$$

up to slowly varying corrections $\sim \ln(r)$.

Calculation of the RCS differential cross section also involves the real part of scattering amplitude, whose relation to the imaginary part is quite straightforward. According to Ref. [35], if the limit $\lim_{s\to\infty}(\frac{\mathcal{I}mf}{s^\alpha})$ exists and is finite, then the real part and imaginary parts of the forward amplitude are related as

$$\mathcal{R}ef(\Delta=0) = s^\alpha \tan\left[\frac{\pi}{2}\left(\alpha-1+\frac{\partial}{\partial \ln s}\right)\right]\frac{\mathcal{I}mf(\Delta=0)}{s^\alpha}. \quad (5)$$

In the model under consideration, the imaginary part of the forward dipole amplitude indeed has a power dependence on energy $\mathcal{I}mf(\Delta=0)(s) \sim s^\alpha$, so (5) simplifies to

$$\frac{\mathcal{R}e\mathcal{A}}{\mathcal{I}m\mathcal{A}} = \tan\left(\frac{\pi}{2}(\alpha-1)\right) \equiv \epsilon. \quad (6)$$

This fixes the phase of the forward Compton amplitude, which we retain for nonzero momentum transfers assuming for the real and imaginary parts similar dependences. Finally we arrive at

$$\mathcal{A}_{\mu\nu} \approx (\epsilon+i) e_\mu^{(i)}(q') e_\nu^{(j)}(q) \int d^2r \int d\beta \bar{\Psi}_\gamma^{(i)}(\beta,r) \times \Psi_\gamma^{(j)}(\beta,r)\,\mathrm{Im} f_{\bar{q}q}^N(\vec{r},\vec{\Delta},\beta,s). \quad (7)$$

For the cross section of unpolarized Compton scattering, from (7) we obtain

$$\frac{d\sigma_{el}^{\gamma p}}{dt} = \frac{1+\epsilon^2}{16\pi}\sum_{ij}|\mathcal{A}_{\mu\nu}^{(ij)}|^2 = \frac{1+\epsilon^2}{16\pi}\sum_{ij}\left|\int d^2r \int d\beta \bar{\Psi}_\gamma^{(i)}(\beta,r)\Psi_\gamma^{(j)}(\beta,r) \times \mathrm{Im} f_{\bar{q}q}^N(\vec{r},\vec{\Delta},\beta)\right|^2. \quad (8)$$

The imaginary part of the forward amplitude (7) gives the total photoabsorption cross section

$$\sigma_{\mathrm{tot}}^{\gamma p} = \frac{1}{16\pi}\int d\beta d^2r |\Psi_\gamma(\beta,r)|^2\,\mathrm{Im} f_{\bar{q}q}^N(\vec{r},\vec{\Delta},\beta). \quad (9)$$

Formulas (8) and (9) are used further for numerical calculations.

III. WAVE FUNCTIONS FROM THE INSTANTON VACUUM

In this section, we present briefly some details of the wave function evaluation in the instanton-vacuum model (see [36–38], and references therein). The central object of the model is the partition function of the light quarks, which has the form

$$Z[v] = \int d\lambda \mathcal{D}\bar{\psi}\mathcal{D}\psi\mathcal{D}\Phi e^{iS[\lambda,v,\bar{\psi},\psi,\Phi]}, \quad (10)$$

where the effective action $S[\lambda, v, \bar{\psi}, \psi, \Phi]$ is defined as [38,39]

$$S[\lambda,v,\bar{\psi},\psi,\Phi] = \int d^4x\left(\frac{N}{V}\ln\lambda + 2\Phi^2(x) - \bar{\psi}(\hat{p}+\hat{v} - m - c\bar{L}f\otimes\Phi\cdot\Gamma_m\otimes fL)\psi\right).$$

Here ψ and Φ are the fields of constituent quarks and mesons, respectively, N/V is the density of the instanton gas, $\hat{v} \equiv v_\mu\gamma^\mu$ is the external vector current corresponding to the photon, L is the gauge factor,

$$L(x,z) = P\exp\left(i\int_z^x d\zeta^\mu v_\mu(\zeta)\right), \quad (11)$$

which provides the gauge covariance of the action, and the nonlinear term in explicit form is

$$-c\bar{\psi}\bar{L}f\otimes\Phi\cdot\Gamma_m\otimes fL\psi \equiv -c\int d^4x d^4y d^4z \bar{\psi}(x) \times \bar{L}(x-z)\tilde{f}(x-z) \times\left(\sum_i \Phi_i(z)\Gamma_{m,i}\right)\tilde{f}(z-y) \times L(z-y)\psi(y), \quad (12)$$

where Γ_m is one of the matrices, $\Gamma_m = \{1, i\vec{\tau}, \gamma_5, i\vec{\tau}\gamma_5\}$, $\tilde{f}(x-y) = \int \frac{d^4p}{(2\pi)^4} f(p) e^{-ip\cdot(x-y)} f(p)$, and $f(p)$ is the Fourier transform of the zero-mode profile.

In the leading order in N_c, we have the same Feynman rules as in the perturbative theory, but with momentum-dependent quark mass $\mu(p)$ in the quark propagator

$$S(p) = \frac{1}{\hat{p} - \mu(p) + i0}. \tag{13}$$

The mass of the constituent quark has a form

$$\mu(p) = m + Mf^2(p),$$

where $m \approx 5$ MeV is the current quark mass and $M \approx 350$ MeV is the dynamical mass generated by the interaction with the instanton-vacuum background. Because of the presence of instantons, the coupling of a vector current to a quark is also modified:

$$\begin{aligned} \hat{v} \equiv v_\mu \gamma^\mu \rightarrow \hat{V} = \hat{v} + \hat{V}^{\text{nonl}}, \\ \hat{V}^{\text{nonl}} \approx -2Mf(p)\frac{df(p)}{dp_\mu} v_\mu(q) + \mathcal{O}(q^2), \end{aligned} \tag{14}$$

where p is the momentum of the incoming quark and q is the momentum of the photon. Notice that for an arbitrary photon momentum q the expression for $\hat{V}^{\text{nonl}}$ depends on the choice of the path in (11), and as a result one can find in the literature different expressions used for evaluations [33,39–41]. In the limit $p \rightarrow \infty$, the function $f(p)$ falls off as $\sim \frac{1}{p^3}$, so for large $p \gg \rho^{-1}$, where $\rho \approx (600\ \text{MeV})^{-1}$ is the mean instanton size, the mass of the quark $\mu(p) \approx m$ and vector current interaction vertex $\hat{V} \approx \hat{v}$. However, we would like to emphasize that the wave function $\Psi(\beta, r)$ gets a contribution from both the soft and the hard parts, so even in the large-Q limit the instanton-vacuum function is different from the well-known perturbative result.

We have to evaluate the wave functions associated with the following matrix elements:

$$\begin{aligned} I_\Gamma(\beta, \vec{r}) = \int \frac{dz}{2\pi} e^{i(\beta+(1/2))q\cdot nz} \langle 0|\bar{\psi}\left(-\frac{z}{2}n - \frac{\vec{r}}{2}\right) \\ \times \Gamma\psi\left(\frac{z}{2}n + \frac{\vec{r}}{2}\right)|\gamma(q)\rangle, \end{aligned} \tag{15}$$

where Γ is one of the matrices $\Gamma = \{\gamma_\mu, \gamma_\mu\gamma_5, \sigma_{\mu\nu}\}$. In the leading order in N_c one can easily obtain

$$\begin{aligned} I_\Gamma = \int \frac{d^4p}{(2\pi)^4} e^{i\vec{p}_\perp\vec{r}_\perp} \delta\left(p^+ - \left(\beta + \frac{1}{2}\right)q^+\right) \\ \times \text{Tr}(S(p)\hat{V}S(p+q)\Gamma). \end{aligned} \tag{16}$$

The evaluation of (16) is quite tedious but straightforward. Details of this evaluation may be found in Ref. [33].

The overlap of the initial and final photon wave functions in (8) was evaluated according to

$$\begin{aligned} \Psi^{(i)*}(\beta, r, Q^2 = 0)\Psi^{(i)}(\beta, r, Q^2) = \sum_\Gamma I^*_\Gamma(\beta, r^*, 0) \\ \times I_\Gamma(\beta, r, Q^2), \end{aligned} \tag{17}$$

where summation is done over possible polarization states $\Gamma = \{\gamma_\mu, \gamma_\mu\gamma_5, \sigma_{\mu\nu}\}$. In the final state we should use $r^*_\mu = r_\mu + n_\mu \frac{q'_\perp \cdot r_\perp}{q_+} = r_\mu - n_\mu \frac{\Delta_\perp \cdot r_\perp}{q_+}$, which is related to the reference frame with $q'_{\perp,\mu} = 0$ in which the components (16) were evaluated.

IV. NUMERICAL RESULTS

A. Photoabsorption

The Bjorken variable used in deep inelastic scattering (DIS), $x = Q^2/(2p \cdot q)$, is not appropriate at small photon virtualities, since it does not have the meaning of a fractional quark momentum any more and may be very small even at low energies. In particular, for RCS the Bjorken variable x defined in this way would be zero. Therefore, one should rely on the phenomenological dipole cross section, which depends on energy, rather than x. We use the s-dependent dipole cross section proposed in [42], which saturates at large separations in analogy to the x-dependent one proposed in [43]. Correspondingly, for the elastic dipole amplitude we employ the model developed in [34,44–46],

$$\begin{aligned} \text{Im}\, f^N_{\bar{q}q}(\vec{r}, \vec{\Delta}, \beta, s) = \frac{\sigma_0(s)}{4} \exp\left[-\left(\frac{B(s)}{2} + \frac{R_0^2(s)}{16}\right)\vec{\Delta}^2_\perp\right] \\ \times (e^{-i\beta\vec{r}\cdot\vec{\Delta}} + e^{i(1-\beta)\vec{r}\cdot\vec{\Delta}} \\ - 2e^{i((1/2)-\beta)\vec{r}\cdot\vec{\Delta}} e^{-((r^2)/(R_0^2(s)))}), \end{aligned} \tag{18}$$

where $\sigma_0(s)$, $R_0^2(s)$, and $B(s)$ are the phenomenological parameters known from DIS and πp scattering data.

We employ the s-dependent parametrization of the dipole cross section suitable for soft processes [42]

$$\sigma_{\bar{q}q}(r, s) = \sigma_0(s)(1 - e^{-r^2/R_0^2(s)}), \tag{19}$$

$$\sigma_0(s) = \sigma_{\pi p}(s)\left(1 + \frac{3}{8}\frac{R_0^2(s)}{r_\pi^2}\right), \tag{20}$$

$$R_0(s) = 0.88\ \text{fm} \times \left(\frac{s_0}{s}\right)^{0.14}, \tag{21}$$

where $s_0 \approx 1000\ \text{GeV}^2$. For the pion cross section we use the parametrization and fit of Ref. [47], namely, its Pomeron part,

$$\sigma_{\pi p}(s) = 23.6\left(\frac{s}{s_0}\right)^{0.079}\ \text{mb}. \tag{22}$$

The parameter $B(s)$ in Eq. (18), is related to the t slope of the differential cross section of elastic πp scattering [44–

46],

$$B(s) = B_{el}^{\pi p}(s) - \tfrac{1}{3}\langle r_{ch}^2\rangle_\pi - \tfrac{1}{8}R_0^2(s). \quad (23)$$

Here we rely on the Regge factorization and use $B_{el}^{\pi p}(s) = B_0 + 2\alpha_P'(0)\ln(s/\mu_0^2)$, with $B_0 = 6\ \mathrm{GeV}^{-2}$, $\langle r_{ch}^2\rangle_\pi = 0.44\ \mathrm{fm}^2$, $\alpha_P'(0) = 0.25\ \mathrm{GeV}^{-2}$, and $\mu_0 = 1\ \mathrm{GeV}$.

This parametrization may be used in Eqs. (8) and (9) only at very high energies where, in terms of the Regge theory, the Pomeron term in the cross section dominates. So far, only two data points shown in Fig. 1 are available for $\sigma_{\gamma p}$ from the H1 and ZEUS experiments [48], and our parameter-free calculation agrees well with these data.

In order to extend the model down to smaller values of $\sqrt{s}$, where more data are available, we added the Reggeon contribution, which was fitted to the photoabsorption data in Ref. [47]:

$$\sigma_{\gamma p}^{(R)}(s) = 129\ \mathrm{nb} \times s^{-0.4525}. \quad (24)$$

Besides, the Pomeron part of the dipole cross section parametrized as in Eqs. (19)–(21) exposes some problems at low energies. Indeed, as one can see from (21), the saturation radius $R_0(s)$ grows and may substantially exceed the confinement radius. In order to regularize the low-energy behavior of $R_0(s)$, we modify Eq. (21) as follows:

$$R_0(s) \Rightarrow \tilde{R}_0(s) = 0.88\ \mathrm{fm}\left(\frac{s_0}{s + s_1}\right)^{0.14}. \quad (25)$$

A fit to low-energy photoabsorption data allows one to fix this parameter at $\sqrt{s_1} = 60$ GeV (see Fig. 1 for more details). Since further evaluations are done in the LHC energy range, the difference between (21) and (25) is negligible, as one can see from Fig. 1. Indeed, both parametrizations coincide for $\sqrt{s} \gtrsim 10$ GeV. In the right pane of Fig. 1, the contributions of the color dipole (9) and Reggeon (24) terms are displayed separately.

B. Compton scattering

Using parametrizations (19)–(22), we calculate the elastic RCS differential cross section as

$$\frac{d\sigma_{el}^{\gamma p}}{dt} = \frac{1+\epsilon^2}{16\pi}\sum_{ij}\left|\int d^2r\int d\beta\bar{\Psi}_\gamma^{(i)}(\beta,r)\Psi_\gamma^{(j)}(\beta,r) \times \mathrm{Im}f_{\bar{q}q}^N(\vec{r},\vec{\Delta},\beta) + 16\pi\sigma_{\gamma p}^{(\mathrm{IR})}(s)e^{B_{\mathrm{IR}}(s)t}\right|^2. \quad (26)$$

Since extraction of Reggeon parameters from experimental data yields huge uncertainties [49], in this paper we rely on the f dominance of the Pomeron [50] and take the Reggeon slope as

$$B_{\mathrm{IR}}(s) = B_1 + 2\alpha_{\mathrm{IR}}'(0)\ln\left(\frac{s}{\mu_0^2}\right), \quad (27)$$

where $B_1 = B_0 = 6\ \mathrm{GeV}^{-2}$, $\alpha_{\mathrm{IR}}'(0) = 0.9\ \mathrm{GeV}^{-2}$, and the results for the differential cross section are presented in Fig. 2. As one can see from the left pane, for $s \gtrsim 10\ \mathrm{GeV}^2$ the cross section rises with energy for small $|t|$ but falls at $|t| = 1\ \mathrm{GeV}^2$. This corresponds to the Regge predicted energy dependence $s^{2(\alpha(t)-1)}$. However, a word of caution is in order here, since the linear t dependence of the Pomeron trajectory may not continue at large $|t|$, and indeed data indicate that $\alpha_P(t)$ levels off [51]. In the right pane of Fig. 2, our predictions for the t dependence of the cross section are plotted for different energies. The cross section demonstrates a shrinkage of diffraction cone with energy in accordance with the Regge theory.

The RCS cross section has been measured so far only at Jefferson Lab (JLAB) at energies $s \lesssim 10\ \mathrm{GeV}^2$ [52]. In Fig. 3, we compare predictions of the color dipole model with experimental data. Since these data also have relatively large $|t| \gtrsim 2\ \mathrm{GeV}^2$ (wide-angle Compton scattering), calculations in the dipole approach go beyond the kinematics of validity of the model. Indeed, Eq. (18), lead

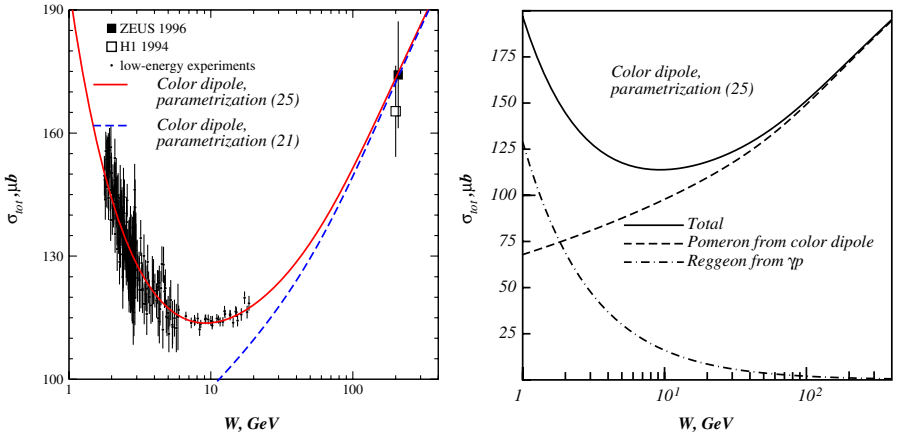

FIG. 1 (color online). Photoabsorption cross section in the color dipole model as a function of c.m. energy $W = \sqrt{s}$. Left: Comparison of calculations with experimental data from ZEUS [48]. The dashed line corresponds to the parametrization (19)–(21), and the solid line corresponds to addition of the Reggeon term [Eq. (25)]. Right: The contributions of the Pomeron and Reggeon parts plotted separately. At $W \gtrsim 10$ GeV. the Reggeon contribution becomes negligibly small.

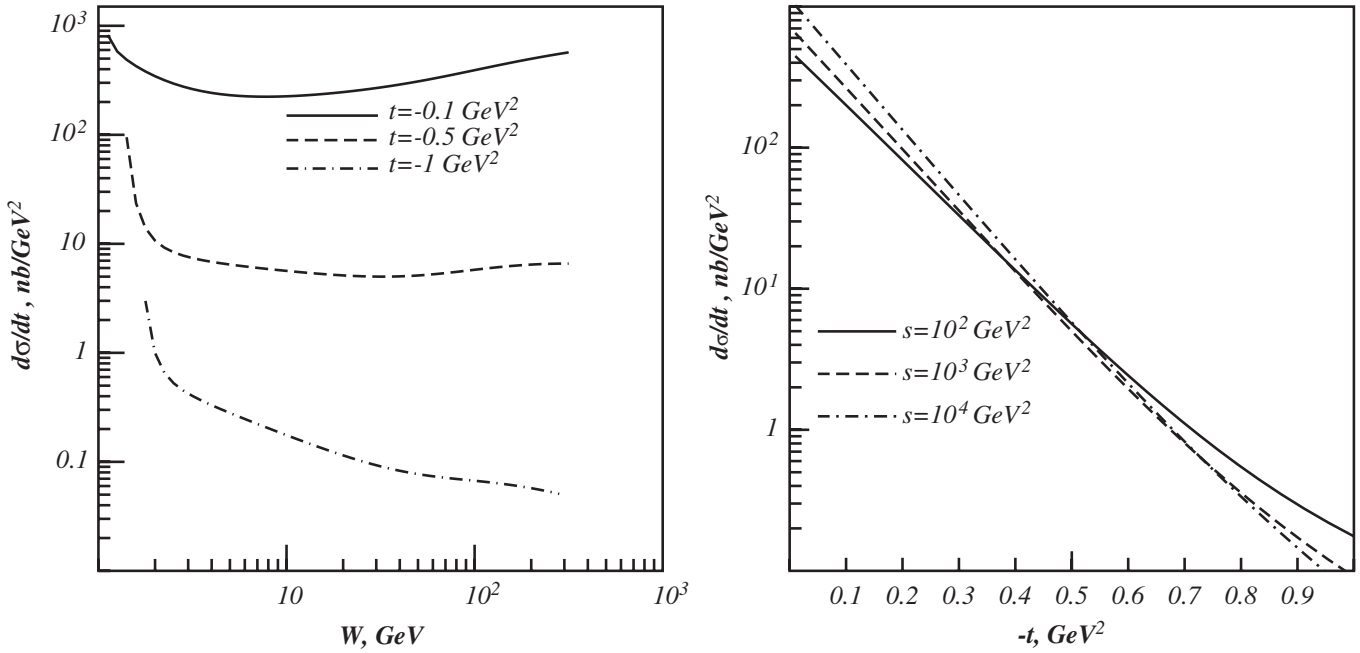

FIG. 2. RCS cross section in the color dipole model. Left: Energy dependence of the RCS cross section for different t, $W \equiv \sqrt{s_{\gamma p}}$. For $s \gtrsim 10$ GeV^2, the cross section depends on the energy s approximately as $s^{2(\alpha(t)-1)}$. For $s \lesssim 10$ GeV^2, we have a "soft" regime where contributions of Reggeons dominate. Right: t dependence of the RCS cross section for different energies in the energy range of ultraperipheral collisions at the LHC.

to the RCS cross section which decreases exponentially at fixed s/t, while the general pQCD analysis [53] predicts $1/s^6$ behavior.

As was discussed in the introduction, there are two approaches which are used to describe the wide-angle Compton scattering. The first one is valid for large $\Delta_\perp$ [18,19] and expresses the amplitude via the distribution amplitude of three valence quarks in the proton. The RCS cross section in this approach was studied in Refs. [16,17], and it was found that evaluation with widely used distribution amplitudes also underestimates the JLAB data [52]. Another description expresses the RCS amplitude via the $1/x$ moment of GPDs at zero skewedness: $\int \frac{dx}{x} H(x, 0, t)$ [5,20,21]. This approach is able to describe the existing JLAB data. However, the t dependence of the cross section

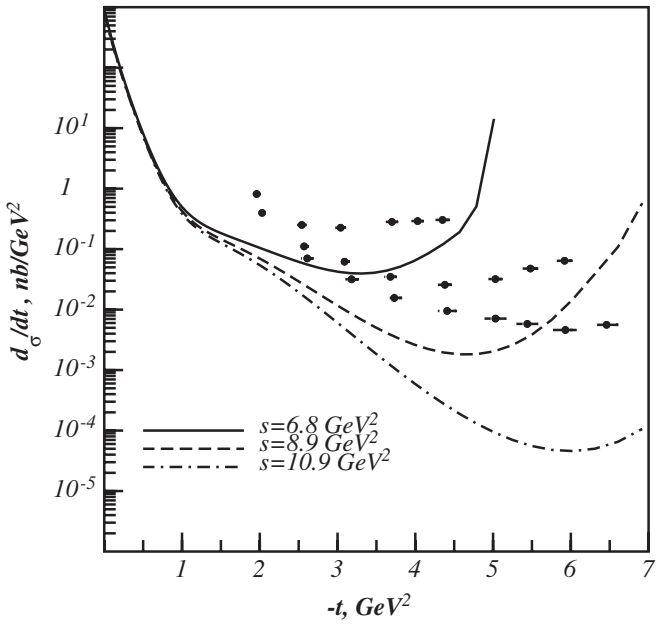

FIG. 3. Comparison of the RCS cross section evaluated in the color dipole model with low-energy (large-angle) experimental data from JLAB [52].

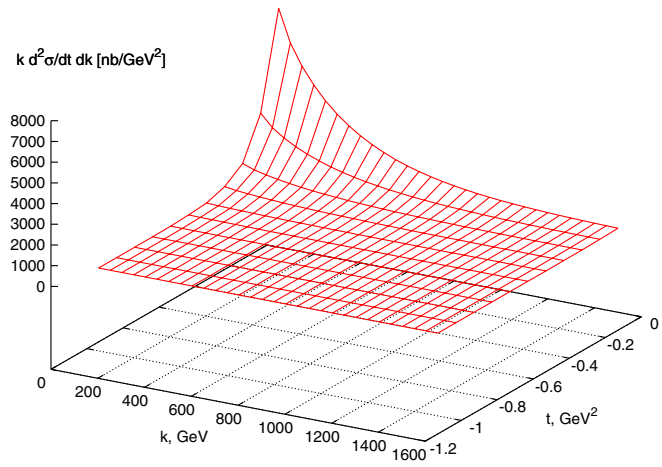

FIG. 4 (color online). Twofold cross section $kd^2\sigma/dtdk$ at the LHC with a c.m. energy $\sqrt{s_{NN}} = 14$ TeV.

in this approach depends on the model for the GPD used in the evaluation.

Since the experimental counting rate also includes the flux of quasireal photons, we present in Fig. 4 the two-dimensional product of the flux and the differential RCS cross section

$$\frac{d^2\sigma_{pp\to pp\gamma}}{dkdt} = \frac{dN_\gamma}{dk}\frac{d\sigma_{\gamma p\to\gamma p}}{dt}, \tag{28}$$

where k is the absolute value of the wave vector of the quasireal photon and photon flux $\frac{dN_\gamma}{dk}$ is given, e.g., in [30].

V. SUMMARY

In this paper, we evaluated the photoabsorption and RCS cross sections within the color dipole model. We employed a photon wave function calculated in the instanton-vacuum model and incorporating nonperturbative effects [33]. For the dipole cross section, we relied on an energy-dependent parametrization, because Bjorken x is not a proper variable at low photon virtualities.

We found that the model describes available data for the photoabsorption cross section from the ZEUS and H1 data quite well, justifying application of the color dipole for processes with real photons. Applicability of the dipole model was extended down to smaller energies $\sqrt{s} \lesssim 30$ GeV by freezing the saturation radius $R_s(s)$ [Eq. (21)] for the energy-dependent parametrization [42], to make sure that it does not exceed the confinement radius.

We also evaluated the RCS cross sections and made predictions for the energy range to be accessed in ultra-peripheral collisions at the LHC (Fig. 2).

ACKNOWLEDGMENTS

This work was supported in part by Fondecyt (Chile) Grants No. 1090291 and No. 1090073 and by DFG (Germany) Grant No. PI182/3-1.

[1] D. Mueller, D. Robaschik, B. Geyer, F. M. Dittes, and J. Horejsi, Fortschr. Phys. **42**, 101 (1994).
[2] X. D. Ji, Phys. Rev. D **55**, 7114 (1997).
[3] X. D. Ji, J. Phys. G **24**, 1181 (1998).
[4] A. V. Radyushkin, Phys. Lett. B **380**, 417 (1996).
[5] A. V. Radyushkin, Phys. Rev. D **56**, 5524 (1997).
[6] A. V. Radyushkin, arXiv:hep-ph/0101225.
[7] X. D. Ji and J. Osborne, Phys. Rev. D **58**, 094018 (1998).
[8] J. C. Collins and A. Freund, Phys. Rev. D **59**, 074009 (1999).
[9] J. C. Collins, L. Frankfurt, and M. Strikman, Phys. Rev. D **56**, 2982 (1997).
[10] S. J. Brodsky, L. Frankfurt, J. F. Gunion, A. H. Mueller, and M. Strikman, Phys. Rev. D **50**, 3134 (1994).
[11] K. Goeke, M. V. Polyakov, and M. Vanderhaeghen, Prog. Part. Nucl. Phys. **47**, 401 (2001).
[12] M. Diehl, T. Feldmann, R. Jakob, and P. Kroll, Nucl. Phys. **B596**, 33 (2001); **B605**, 647(E) (2001).
[13] A. V. Belitsky, D. Mueller, and A. Kirchner, Nucl. Phys. **B629**, 323 (2002).
[14] M. Diehl, Phys. Rep. **388**, 41 (2003).
[15] A. V. Belitsky and A. V. Radyushkin, Phys. Rep. **418**, 1 (2005).
[16] A. S. Kronfeld and B. Nizic, Phys. Rev. D **44**, 3445 (1991); **46**, 2272(E) (1992).
[17] T. C. Brooks and L. J. Dixon, Phys. Rev. D **62**, 114021 (2000).
[18] G. P. Lepage and S. J. Brodsky, Phys. Lett. **87B**, 359 (1979).
[19] G. P. Lepage and S. J. Brodsky, Phys. Rev. D **22**, 2157 (1980).
[20] M. Diehl, T. Feldmann, R. Jakob, and P. Kroll, Eur. Phys. J. C **8**, 409 (1999).
[21] M. Diehl, T. Feldmann, R. Jakob, and P. Kroll, Eur. Phys. J. C **39**, 1 (2005).
[22] M. Klein and P. Newman, CERN Courier **49N3**, 22 (2009).
[23] LHeC website http://www.ep.ph.bham.ac.uk/exp/LHeC/.
[24] EIC website http://www.phenix.bnl.gov/WWW/publish/abhay/Home_of_EIC/.
[25] EIC White paper http://www.phenix.bnl.gov/WWW/publish/abhay/Home_of_EIC/NSAC2007/070424_EIC.pdf.
[26] B. I. Abelev *et al.* (STAR Collaboration), Phys. Rev. C **77**, 034910 (2008).
[27] J. Adams *et al.* (STAR Collaboration), Phys. Rev. C **70**, 031902 (2004).
[28] C. Adler *et al.* (STAR Collaboration), Phys. Rev. Lett. **89**, 272302 (2002).
[29] D. G. d'Enterria, arXiv:nucl-ex/0601001.
[30] K. Hencken *et al.*, Phys. Rep. **458**, 1 (2008).
[31] B. Z. Kopeliovich, L. I. Lapidus, and A. B. Zamolodchikov, Pis'ma Zh. Eksp. Teor. Fiz. **33**, 612 (1981) [JETP Lett. **33**, 595 (1981)].
[32] A. H. Mueller, Nucl. Phys. **B335**, 115 (1990); A. H. Mueller and B. Patel, Nucl. Phys. **B425**, 471 (1994).
[33] A. E. Dorokhov, W. Broniowski, and E. Ruiz Arriola, Phys. Rev. D **74**, 054023 (2006).
[34] B. Z. Kopeliovich, I. Schmidt, and M. Siddikov, Phys. Rev. D **79**, 034019 (2009).
[35] J. B. Bronzan, G. L. Kane, and U. P. Sukhatme, Phys. Lett. **49B**, 272 (1974).
[36] T. Schafer and E. V. Shuryak, Rev. Mod. Phys. **70**, 323 (1998).
[37] D. Diakonov and V. Y. Petrov, Nucl. Phys. **B272**, 457 (1986).
[38] D. Diakonov, M. V. Polyakov, and C. Weiss, Nucl. Phys. **B461**, 539 (1996).

[39] K. Goeke, M. M. Musakhanov, and M. Siddikov, Phys. Rev. D **76**, 076007 (2007).
[40] I. V. Anikin, A. E. Dorokhov, and L. Tomio, Fiz. Elem. Chastits At. Yadra **31**, 1023 (2000) [Phys. Part. Nucl. **31**, 509 (2000)].
[41] A. E. Dorokhov and W. Broniowski, Eur. Phys. J. C **32**, 79 (2003).
[42] B. Z. Kopeliovich, A. Schfer, and A. V. Tarasov, Phys. Rev. D **62**, 054022 (2000).
[43] K. J. Golec-Biernat and M. Wusthoff, Phys. Rev. D **59**, 014017 (1998).
[44] B. Z. Kopeliovich, H. J. Pirner, A. H. Rezaeian, and I. Schmidt, Phys. Rev. D **77**, 034011 (2008).
[45] B. Z. Kopeliovich, A. H. Rezaeian, and I. Schmidt, Phys. Rev. D **78**, 114009 (2008).
[46] B. Z. Kopeliovich, I. K. Potashnikova, I. Schmidt, and J. Soffer, Phys. Rev. D **78**, 014031 (2008).
[47] A. Donnachie and P. V. Landshoff, Phys. Lett. B **296**, 227 (1992).
[48] S. Chekanov *et al.* (ZEUS Collaboration), Nucl. Phys. **B627**, 3 (2002).
[49] A. Aktas *et al.* (H1 Collaboration), Eur. Phys. J. C **48**, 749 (2006).
[50] A. C. Irving, Nucl. Phys. **B121**, 176 (1977).
[51] A. Brandt *et al.* (UA8 Collaboration), Nucl. Phys. **B514**, 3 (1998).
[52] A. Danagoulian *et al.* (Hall A Collaboration), Phys. Rev. Lett. **98**, 152001 (2007).
[53] S. J. Brodsky and G. R. Farrar, Phys. Rev. Lett. **31**, 1153 (1973).